tvst

DOI: 10.1167/tvst.6.6.9

Article

Agreement in Cone Density Derived from Gaze-Directed Single Images Versus Wide-Field Montage Using Adaptive Optics Flood Illumination Ophthalmoscopy

Avenell L. Chew[1,2,*], Danuta M. Sampson[1,2,*], Irwin Kashani[2,3], and Fred K. Chen[1,2,4]

[1] Centre for Ophthalmology and Visual Science, The University of Western Australia, Perth, Western Australia, Australia
[2] Ocular Tissue Engineering Laboratory, Lions Eye Institute, Perth, Western Australia, Australia
[3] Save Sight Institute, The University of Sydney, Sydney, New South Wales, Australia
[4] Department of Ophthalmology, Royal Perth Hospital, Perth, Western Australia, Australia

Correspondence: Fred K. Chen, Lions Eye Institute, 2 Verdun Street, Nedlands WA, Australia. e-mail: fredchen@lei.org.au

Received: 18 April 2017
Accepted: 25 October 2017
Published: 22 December 2017

Keywords: rtx1 adaptive optics camera; retinal imaging; preferred retinal locus; foveal center; clinical trials endpoint

Citation: Chew AL, Sampson DM, Kashani I, Chen FK. Agreement in cone density derived from gaze-directed single images versus wide-field montage using adaptive optics flood illumination ophthalmoscopy. Trans Vis Sci Tech. 2017;6(6):9, doi: 10.1167/tvst.6.6.9

Purpose: We compared cone density measurements derived from the center of gaze-directed single images with reconstructed wide-field montages using the rtx1 adaptive optics (AO) retinal camera.

Methods: A total of 29 eyes from 29 healthy subjects were imaged with the rtx1 camera. Of 20 overlapping AO images acquired, 12 (at 3.2°, 5°, and 7°) were used for calculating gaze-directed cone densities. Wide-field AO montages were reconstructed and cone densities were measured at the corresponding 12 loci as determined by field projection relative to the foveal center aligned to the foveal dip on optical coherence tomography. Limits of agreement in cone density measurement between single AO images and wide-field AO montages were calculated.

Results: Cone density measurements failed in 1 or more gaze directions or retinal loci in up to 58% and 33% of the subjects using single AO images or wide-field AO montage, respectively. Although there were no significant overall differences between cone densities derived from single AO images and wide-field AO montages at any of the 12 gazes and locations ($P = 0.01$–0.65), the limits of agreement between the two methods ranged from as narrow as −2200 to +2600, to as wide as −4200 to +3800 cones/mm^2.

Conclusions: Cone density measurement using the rtx1 AO camera is feasible using both methods. Local variation in image quality and altered visibility of cones after generating montages may contribute to the discrepancies.

Translational Relevance: Cone densities from single AO images are not interchangeable with wide-field montage derived–measurements.

Introduction

In vivo cellular imaging of the human retina is achieved by incorporation of adaptive optics (AO) technology into clinical ophthalmic imaging devices. Through measurement and instantaneous compensation of wavefront distortions caused by ocular aberrations, AO devices improve resolution so as to make possible visualization of individual cone photoreceptor outer segments. Currently, several studies are registered on the clinicaltrials.gov website that use AO retinal imaging to measure secondary endpoints (NCT02317328, NCT02828215, NCT02826655, NCT01866371, NCT00254605, NCT02889185, NCT01846052, NCT02714816). However, there is no consensus on either the optimal methods of postacquisition image processing or the selection of sampling windows for cone density measurements.

Macular diseases may present with multiple lesions that vary in size, number, and location between eyes or patients. While AO cameras have been shown to capture images successfully from the same retinal area over follow-up visits to follow progression of lesions with excellent accuracy in patients with stable foveal fixation,[1] there often are a number of retinal lesions in

several retinal areas that should be tracked over time, and fixation locus may drift due to foveal involvement by the lesion. Therefore, single AO images of 4° × 4° field size, derived from the current commercially available flood-illumination ophthalmoscopy system, the rtx1 camera, are inadequate for documenting macular disease severity or progression. To visualize photoreceptors in the entire macular region, multiple AO images with overlapping regions are required to create a wide-field AO montage.[2] However, this process is time- and labor-intensive. Furthermore, commercial cone analysis software (AODetect; Imagine Eyes, Orsay, France) can process only the raw 4° × 4° single AO images and not the reconstructed wide-field AO montage. The effort and time required for postprocessing is even greater for images from an AO scanning laser ophthalmoscopy (SLO) system where the field size can be smaller than 1° × 1°. Hence, several previous studies have used single AO images showing regions of interest by directing the patient's gaze through an internal fixation target.[3–5] Subsequent single AO images taken with the same gaze direction are used for monitoring progression at the same retinal location. However, fixation drift, microsaccades, and other factors that affect fixation stability and location potentially can alter the exact retinal location imaged through gaze-directed techniques. Therefore, it cannot be assumed that the cone density derived from the center of a gaze-directed single AO image is interchangeable with cone density measurement at the corresponding field-determined retinal location relative to the foveal center in a wide-field AO montage.

To determine whether the cone density measurements derived from these two methods of selecting sampling windows are comparable, we compared the cone photoreceptor densities calculated from the center of single AO images derived from 12 gaze directions to that calculated from the corresponding field-determined retinal locations from the wide-field AO montage from the same eye in a healthy cohort.

Methods

Human Subjects

This research followed the tenets of the Declaration of Helsinki, and was approved by The University of Western Australia human research ethics committee (RA/4/1/7226). Healthy subjects were recruited from the retinal clinic at Lions Eye Institute.

Inclusion criteria were normal ocular examination, best-corrected visual acuity of greater than 80 letters on the Early Treatment Diabetic Retinopathy Study (ETDRS) chart, and ability to give informed consent. Subjects with a history of any ocular surgery, use of medications that potentially may affect photoreceptors (for example hydroxychloroquine, antipsychotics, and tamoxifen), any media opacity, and refractive errors of greater than −6.0 diopters (D) of myopia, greater than +4.0 D of hyperopia, or 4.0 D of astigmatism were excluded. Patients with any abnormality on macular spectral-domain optical coherence tomography (SD OCT) and fundus autofluorescence (FAF) imaging also were excluded (as determined by the senior author, FKC).

Clinical Evaluation

Visual acuity was measured on the ETDRS letter chart and dilated fundus examination was performed by the senior author (FKC). All patients underwent macular FAF imaging and SD OCT combined with near-infrared reflectance (Spectralis, Heidelberg Engineering, Heidelberg, Germany) of the macular region (25° × 30°) and peripapillary nerve fiber layer to exclude subclinical macular or optic nerve pathology. Subjective refraction was performed to determine refractive error. Axial length and corneal curvature measurements were obtained from IOLMaster500 (Carl Zeiss Meditec, Dublin, CA).

Imaging the Human Photoreceptor Mosaic

The photoreceptor outer segment mosaic was imaged using an AO flood illumination ophthalmoscope (AO-FIO; rtx1; Imagine Eyes). The 4° × 4° single AO image is derived from 40 raw image frames acquired within 4 seconds. The onboard software discards frames with poor quality and averages the remaining frames to improve the signal-to-noise ratio of the image to improve the visibility of cone reflexes. The final image corresponds to a region of approximately 4° × 4° (750 × 750 pixels – oversampled to 1500 × 1500 pixels) or 1200 × 1200 μm in area. A total of 20 consecutive single images with 1° to 2° of overlap were used to create the wide-field AO montage (Fig. 1).

Since the resolution of the system is 250 line pairs per mm, structures with a diameter of less than 2 μm cannot be resolved and, thus, foveal cones cannot be visualized adequately. Consequently, we have chosen to examine only cone densities at retinal loci from 3° to 7° of eccentricity. The 12 chosen gaze directions and retinal locations are shown in Figure 1.

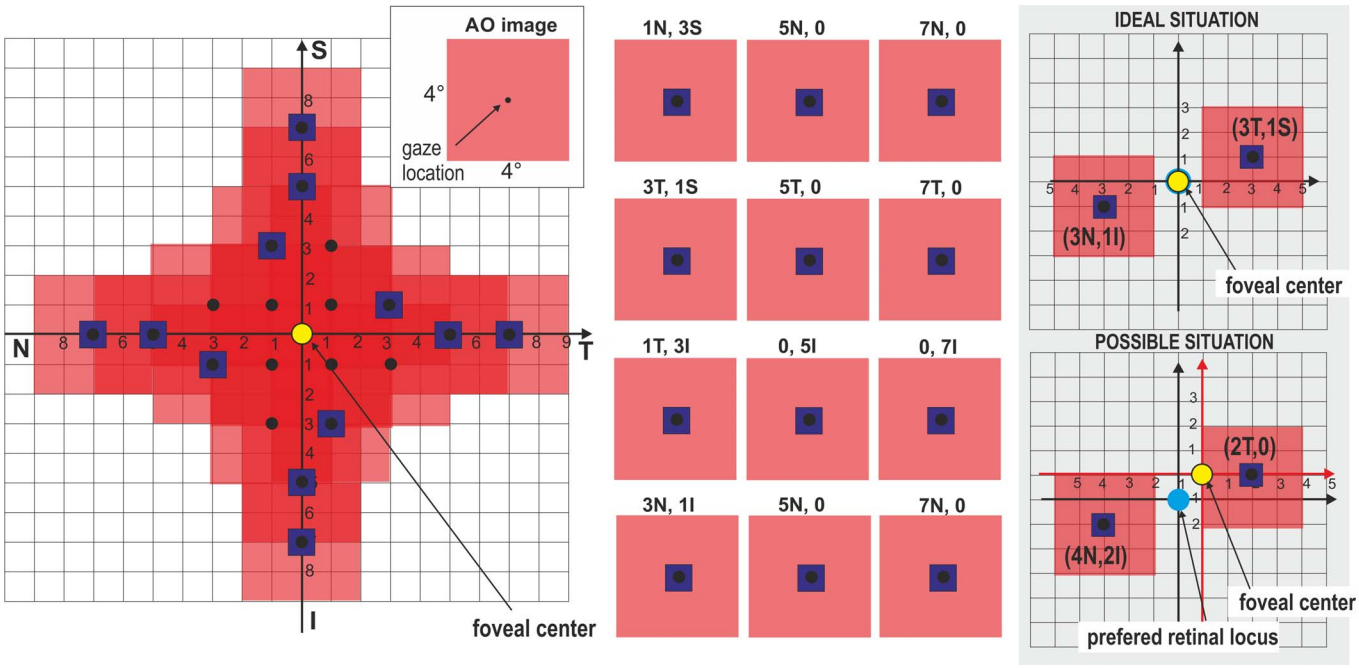

Figure 1. *Left*: 20 AO image frames, each measuring 4° × 4°, are acquired at the coordinates marked by the *black dots*, to cover the area of retina shown in *red*. Areas of overlap between AO frames are depicted by the darker shades of *red*. The 12 loci studied here are shown by the *blue boxes*. *Center*: For analysis of single AO frames, the internal target in the AO device is set at each of the 12 coordinates of interest, and the sampling windows are extracted from the center of each AO frame. *Right*: In the ideal situation, the position of a gaze-directed single AO frame exactly matches its retinal location relative to the anatomical fovea (*top*). It is possible that the positon of the preferred retinal locus (*blue dot*) does not match the position of the anatomical fovea (*yellow dot*), so that the actual position of the single AO frame is translated relative to the intended coordinates being studied.

Cone Density from Gaze-Directed Single AO Images

The cone densities in the middle of single AO images from the 12 gaze directions were calculated. With the knowledge that each single AO image of 1500 × 1500 pixels covers an area of 4° × 4° of the retina and of the axial length, the μm/pixel equivalent (scaling factor) is calculated from axial length based on a modification of Littmann's formula by Bennett et al.[6] as follows:

$$\text{Scaling factor} = \frac{1000}{1500} \times 4 \times 0.01306 \times (\text{axial length in mm} - 1.82).$$

Five overlapping sampling windows of 50 × 50 μm located at the center of each of the 12 gaze-directed single AO images were cropped for automated cone counting (Fig. 2). These sampling windows underwent further image processing to enhance the signal-to-noise ratio according to methods described previously,[7] and the number of cones was counted using automated custom software based on the circle Hough transform, as described previously by our group.[7]

The quality of the images from the sampling windows was determined by an experienced observer (DMS) and those that subjectively were deemed too poor for accurate cone density measurement were excluded from further analysis. The remaining sampling windows were processed and the one with the highest cone photoreceptor count was used to derive the cone density. A total of 5 × 12 × 29 = 1740 sampling windows from single AO images were graded and 750 (43%) were discarded due to poor image quality.

Cone Density from field-Determined Retinal Location on Wide-Field AO Montage

Overlapping single AO images were stitched together to reconstruct the wide-field AO montage by using the MosaicJ plugin[8] for ImageJ (Laboratory for Optical and Computational Instrumentation, Madison, WI). The semiautomated process of creating a montage involves manually bringing one single image at a time to merge with the growing montage. If no overlapping regions are identified in the next single image, subsequent images also are examined and merged with the growing montage. Once the montage

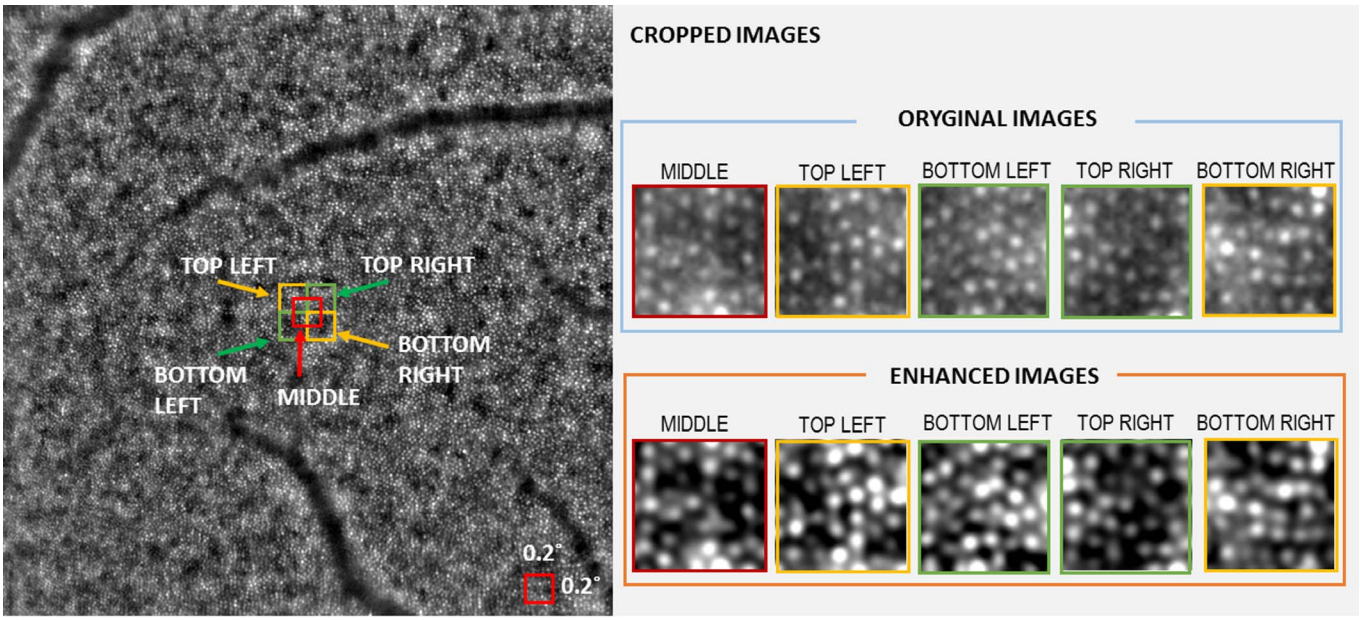

Figure 2. At each retinal locus, five sampling windows each measuring 50 × 50 μm were extracted, enhanced, and analyzed to determine the cone density at that region.

is created manually, an automated process refines the alignment by translation and rotation but without magnification. The boundaries of overlapping images are blended to reduce visibility of image edges.

The location of the foveal center in the wide-field AO montage is determined through alignment with a high quality 30° near-infrared reflectance (NIR) image using Adobe Photoshop CS6 (Adobe Systems, Inc., San Jose, CA). Using this software, the NIR image is transformed with respect to the montage using vessel landmarks to coregister the images. This preserves the pixel size of the wide-field montage. However, rotational transformations are performed on the montage so that the NIR image remains square. The NIR image also is coregistered with a single horizontal SD OCT scan that cuts across the foveal center so that the location of the foveal dip can be marked on the NIR image (Fig. 3). The alignment between the marked NIR image and the wide-field AO montage allows the foveal center to be determined on the AO montage. The actual size of the 30° NIR fundus image obtained using the Spectralis device can vary between patients, as it depends on magnification related to axial length.[9,10] The retinal magnification factor for each eye was calculated from axial length measured by IOLMaster 500 according to the modified Littmann's method described by Bennett et al., $q = 0.01306 \times (\text{axial length} - 1.82)$ where q is the magnification factor for that eye.[6]

A calibrated Cartesian grid consisting of 1° × 1° squares then is overlaid onto the montage with its center at the marked anatomical fovea and horizontal meridian aligned with the horizontal SD OCT scan. This then allows accurate localization of the angular coordinates of the 12 loci relative to the marked fovea on the wide-field montage.

The five sampling windows of 50 × 50 μm at each of the 12 study loci identified by the Cartesian grid overlay on the wide-field AO montage were cropped for automated cone counting (Fig. 2). The further image-processing, cone counting, and the quality image assessment were subjected to identical procedures as single AO images that are described above. A total of $5 \times 12 \times 29 = 1740$ sampling windows from wide-field AO montage were graded and 690 (40%) were discarded due to poor image quality.

Statistical Analysis

The number of study loci that had inadequate image quality (for all 5 overlapping sampling windows) was recorded for each subject for each method of selecting sampling windows. Association between the method of sampling (single AO image vs. wide-field AO montage) and adequate image quality was examined by the McNemar test. Means and standard deviations of the differences between gaze-directed and field-determined cone densities for each of the retinal loci were calculated. Paired *t*-

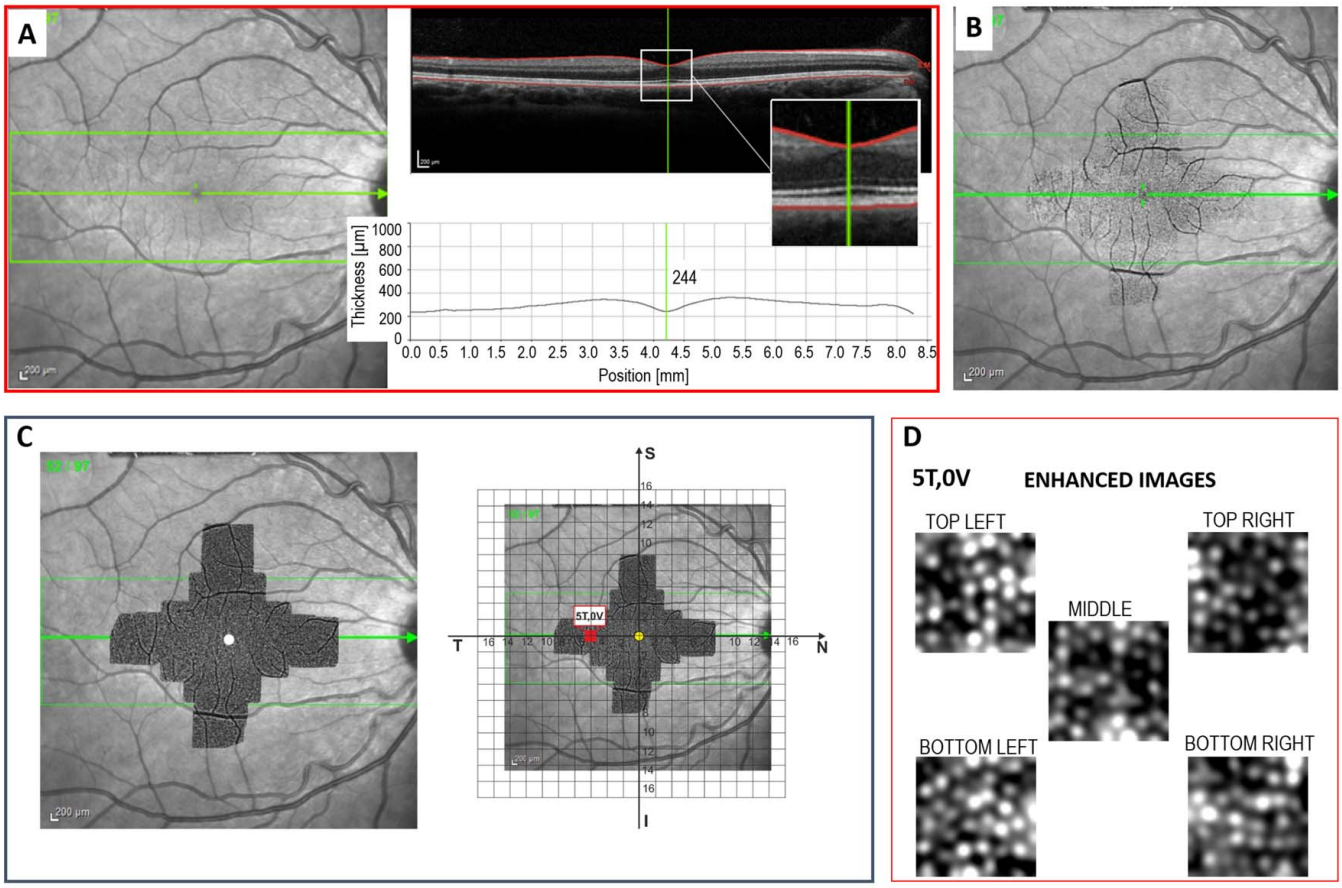

Figure 3. The anatomical foveal center is identified as that position on the OCT volume scan at which the minimum retinal thickness occurs (A). The anatomical fovea then is marked on the NIR fundus image (B) and the AO montage is overlaid on the marked fundus image. A grid consisting of $1° \times 1°$ squares is superimposed onto the final image to identify the retinal loci of interest relative to the fovea (C). Five sampling windows are extracted from each retinal locus and the images are enhanced before being analyzed (D).

testing was used to compare mean cone density at each locus. A scatter of absolute differences between gaze-directed and field-determined cone densities against the average counts was plotted and Kendell correlation coefficient (Tau) was calculated to confirm that there was no relationship between the differences and mean. If this condition was preserved, then Bland-Altman analyses were performed at each of the 12 retinal loci, and 95% limits of agreement were calculated. Null hypothesis was rejected if the P value was less than 0.05.

Results

Demographics

A total of 29 eyes of 29 subjects (16 males and 13 females; median age, 62 years; range, 21–70 years) were examined. Mean (standard deviation) visual acuity score was 90 letters (3.8) and median (range) spherical equivalent refractive error and axial lengths were 0.00 D (−4.75, +2.75) D and 23.99 (22.56, 25.59) mm.

Feasibility in Cone Density Measurement

Mean numbers of subjects contributing to cone density measurement across all study loci was 27 (range, 21–29) and 26 (range, 23–29) for wide-field AO montage and single AO image respectively (Table 1). Only 13/29 (45%) subjects contributed to cone density measurements at all 12 study loci from both sampling methods (Table 2). For the remaining 16/29 (55%) subjects, up to seven study loci from either the single AO image or the wide-field AO montage sampling windows were of inadequate image quality

Table 1. Mean and Median Cone Density for Each Gaze Direction or Retinal Location

Location (H, V)	Number of Subjects		Cone Photoreceptor Cell Density, Cones/mm^2					
			Mean		Median		Range	
	AO Montage	AO Image	AO Montage	AO Image	AO Montage	AO Image	AO Montage	AO Image
1N, 3S	29	28	18,900	18,200	18,000	18,000	15,800–20,000	15,700–20,800
3N, 1I	28	25	18,900	18,400	18,800	18,300	14,800–22,700	14,600–21,700
1T, 3I	27	28	17,400	17,600	17,200	17,600	15,800–20,400	13,500–22,200
3T, 1S	29	27	18,400	17,500	18,400	17,500	15,200–21,300	13,700–22,000
5N, 0	28	28	17,800	17,300	17,700	17,300	15,000–21,700	14,400–19,500
5T, 0	29	27	17,500	17,000	17,500	16,800	15,000–21,000	13,900–19,800
0, 5S	29	26	16,500	15,900	16,500	15,800	13,200–18,700	12,800–20,400
0, 5I	25	26	16,200	16,000	16,400	15,400	13,200–19,200	13,600–19,100
7N, 0	25	24	15,300	14,500	15,600	14,600	13,100–18,700	11,800–16,700
7T, 0	26	28	15,200	14,600	14,800	14,300	12,100–17,800	11,700–16,900
0, 7S	28	23	14,700	14,300	14,400	14,600	11,700–17,200	12,200–18,000
0, 7I	21	24	14,000	14,100	14,100	14,000	11,800–17,000	11,700–16,700

N, nasal; T, temporal; I, inferior; S, superior; H, horizontal coordinate; V, vertical coordinate.

for cone density measurements (Table 2). Although a greater proportion of the cohort had adequate image quality sampling windows at all 12 study loci when single AO images were used (62%) compared to wide-field AO montages (52%), this was not statistically significantly different ($\chi^2 = 0.571$, df = 1, $P = 0.45$). Failure to obtain adequate image quality in the sampling windows occurred even in younger subjects (Subjects 6, 15, 16) despite relatively mild refractive error (Subject 15).

Agreement Between Single AO Image and Wide-Field AO Montage Derived Cone Densities

Mean cone densities calculated from the single AO images at each of the 12 retinal loci are shown in Table 1. As expected, cone density decreased with increasing eccentricity. Bland-Altman plots were generated for each retinal locus and none showed a relationship between differences and magnitude (Fig. 4, Supplementary Fig. S1). Limits of agreement between cone densities derived from the 12 gaze-directed single AO images and the 12 retinal locations on the wide-field AO montages are shown in Table 3. The number of eyes available for calculating limits of agreement diminished with increasing eccentricity of the study locus. The estimated bias in cone density (single AO image–derived cone density minus wide-field AO montage–derived cone density) varied from −900 to +200 cones/mm^2. Although there was a trend for higher cone density derived from wide-field AO montages compared to single AO images, this was not statistically significant for each of the 12 study loci (Table 3). The best agreement was observed at the retinal locus of 0° nasal and 7° inferior where the lower and upper limits of agreement were –2200 and +2600 cones/mm^2, respectively. The greatest disagreement was observed at the retinal locus of 0° nasal and 5° inferior where the lower and upper limits of agreement were –4200 and +3800 cones/mm^2, respectively.

Illustrative Cases

Examples of the actual differences in cone density derived from gaze-directed and field-determined retinal sampling windows are illustrated in three subjects as shown in Figure 5. There was significant displacement between the center of single AO images as determined by gaze direction and the actual position of the retinal locus as determined by field projection on wide-field AO montages. The image quality and number of visualized cones varied between the sampling windows obtained from these methods (Table 4). There was a trend for greater cone density in the sampling window extracted from the wide-field AO montages compared to single AO images but this reached significance for only one of the three subjects.

Table 2. Frequency of Missing Data on Cone Density Measurement due to Poor Image Quality for Each or Both Sampling Methods

Subject ID	Age, y	Refractive Error, D	Single AO Image	Widefield AO Montage	Both Methods
1	67	−1.00	0	1	0
2	29	−0.50	0	0	0
3	68	1.75	1	1	0
4	64	0.25	0	0	0
5	57	0.25	0	0	0
6	32	−3.50	4	2	0
7	58	0.88	0	3	0
8	69	−1.75	0	1	0
9	70	2.75	0	0	0
10	70	2.25	5	1	1
11	69	−0.13	4	3	3
12	65	2.00	0	0	0
13	75	0.75	0	2	0
14	65	1.88	1	0	0
15	22	0.00	3	1	1
16	21	−4.75	3	2	2
17	54	0.50	0	0	0
18	68	−0.25	0	1	0
19	49	−0.25	0	0	0
20	52	−0.13	0	0	0
21	54	0.00	0	0	0
22	58	−3.25	0	0	0
23	44	0.13	0	0	0
24	70	1.00	1	0	0
25	62	−1.38	3	1	0
26	62	0.75	7	4	4
27	59	−0.50	0	0	0
28	53	1.25	2	1	1
29	25	−3.25	0	0	0
Average	55.6	−0.15	1.2	0.8	0.5

Discussion

Our study provides the estimated limits of agreement between cone densities derived from gaze-directed single AO frames and those obtained from field-determined localization on wide-field AO montages. Although there was no statistically significant difference in cone densities derived from the two methods, the limits of agreement were relatively wide. These findings have significant implications on the comparability of cone density values from clinical trials that use different methodologies to sample the area of interest for cone density measurement.

The proportions of sampling windows that were discarded before analysis due to poor image quality were 43% when taken from single AO image frames, and 40% when taken from the wide-field AO montages. Debellemanière et al.[11] reported exclusion of at least one eye from 46.9% of subjects due to inadequate AO image quality in their study of patients taking hydroxychloroquine without any evidence of maculopathy. Further, in a separate study of AO images obtained from 72 eyes of healthy subjects aged 14 to 69 years, the images from 52.7% of subjects were excluded from analysis due to image quality that was insufficient to allow automatic montage and/or cone counting, including two patients who were aged under 30 with no apparent ocular pathology.[12] Both studies used the same commercial instrument for AO image acquisition as the one used in our study. It is unclear what causes these relatively high rates of sampling window failing image quality control, given that factors known to cause difficulty with AO imaging, such as macular pathology, media opacity, and extremes of refractive errors, have been excluded from the study population. It is possible that a number of higher order aberrations are not corrected adequately or perhaps not corrected at all using this instrument in a significant proportion of people. The variability in obtaining adequate quality AO images in healthy subjects is not limited to flood-illumination optical devices. Using AO-SLO, Li et al.[13] were able to resolve the entire foveal cone mosaic in just four of 18 healthy eyes with varying axial lengths, mostly due to failure to obtain adequate images within 0.03 mm eccentricity of the center of the fovea. Improvements to hardware-based adaptive optics may improve our ability to correct for the eye's wave aberrations, but there also are computational wavefront correction algorithms that have enabled visualization of even highly packed individual cone photoreceptors without the need for expensive, bulky hardware.[14–16] In the foreseeable future, computational correction of images may augment or even replace hardware-based adaptive optics technologies in visualizing human retinal photoreceptor cells.

We demonstrated a misalignment of up to 2° between retinal loci defined by gaze direction and the corresponding field projected retinal loci in three eyes from three randomly selected healthy subjects. In the first and third cases shown, this translation is temporal, whereas in the second case, the translation is nasal and the magnitude of the translation is

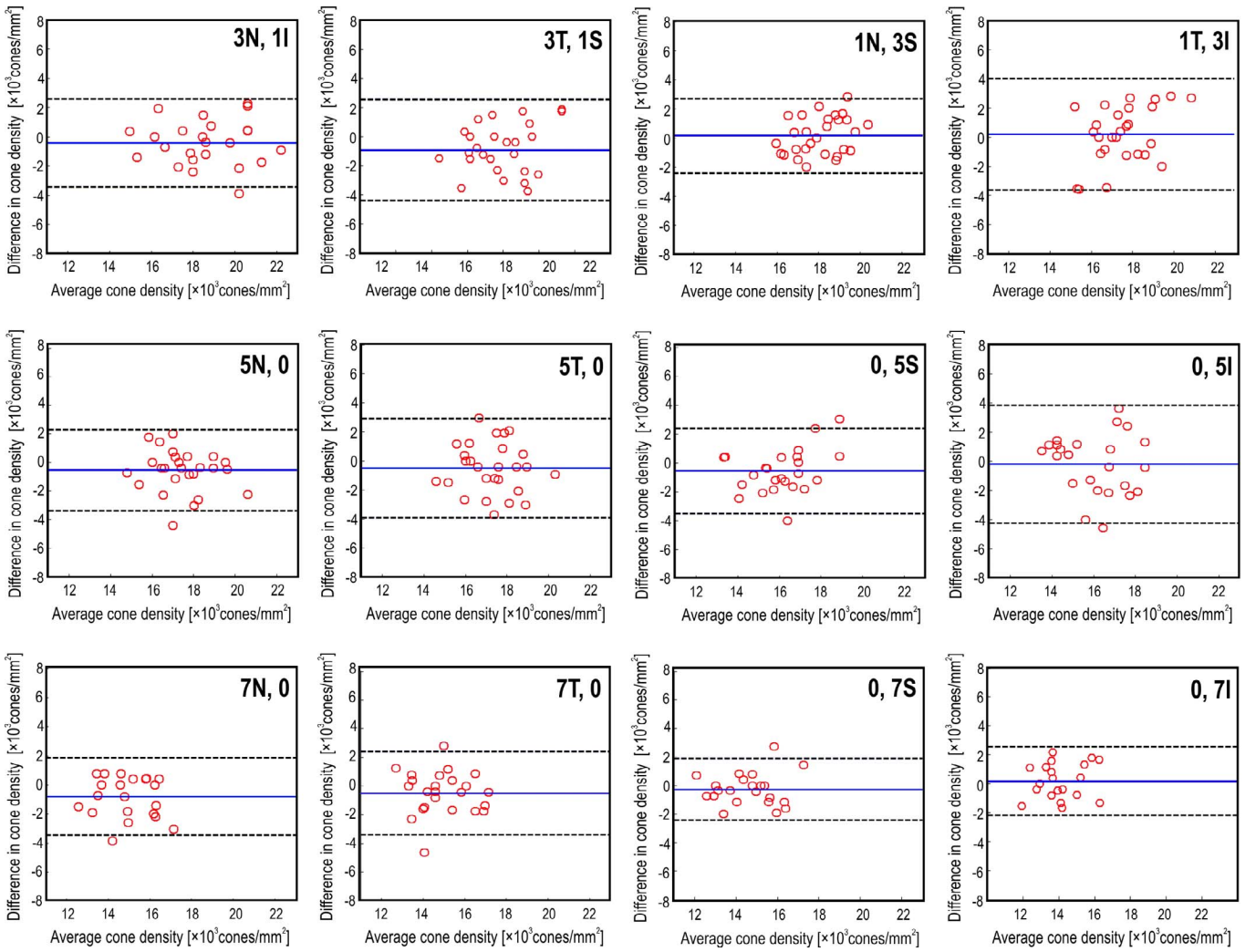

Figure 4. Bland-Altman plots at all 12 retinal loci with mean difference (single AO image derived cone density minus wide-field AO montage derived cone density) indicated by *solid blue line*, limits of agreement by the *dashed black lines*.

variable between the subjects and loci. Several studies have described the relationship between fixationally- and anatomically-determined retinal loci using structural modalities other than OCT to identify the fovea centralis. These include AO cone photoreceptor imaging to identify the position at which the greatest peak of cone density occurs[17–19] and fluorescein angiography to identify the central point of the foveal avascular zone.[20] They show that the location of the anatomically-determined fovea center often does not correlate precisely with the centroid of the preferred retinal locus and that the magnitude of the misalignment in these retinal locations varies between subjects. It also has been shown that the center of fixation is displaced from the location of peak foveal cone density as measured by AO imaging by an average of 18 to 34 μm.[17–19] Micro-saccades also contribute to the mismatch of retinal locations between the gaze-directed and anatomically-determined loci of interest. In healthy subjects, it has been estimated that the standard deviation of intertrial fixation position is approximately 17 μm in each of the horizontal and vertical directions.[17,21,22] Theoretical calculations performed previously by Lombardo et al.[23] estimate that the magnitude of the error resulting from displacing the sampling window 18 μm along the horizontal meridian at an eccentricity of approximately 4.3° would be less than 500 cones/mm^2, and that the error is greater towards the foveal center, but still is less than 1000 cones/mm^2 at $<1°$ eccentricity. Therefore, we have designed a prospective study to examine the actual differences in cone density measurements resulting from shift in region of interest due to different sampling methods.

Table 3. Limits of Agreement between Cone Densities Derived from Single AO Images Compared to Wide-Field AO Montages

Location (H, V)	Number of Subjects	Cone Photoreceptor Cell Density Comparison, Cones/mm^2 Gaze vs. Field			
		Mean Difference[a]	SD	Limits of Agreement[b] (lower bound, upper bound)	*P* Value*
1N, 3S	28	+200	1300	−2400,+2700	0.51
3N, 1I	24	−400	1500	−3400,+2600	0.18
1T, 3I	27	+200	1900	−3600,+4000	0.60
3T, 1S	27	−900	1800	−4400,+2500	0.01
5N, 0	27	−500	1500	−3400,+2300	0.07
5T, 0	27	−500	1700	−3900,+2900	0.15
0, 5S	25	−500	1500	−3500,+2400	0.11
0, 5I	24	−200	2100	−4200,+3800	0.65
7N, 0	23	−800	1400	−3500,+1900	0.01
7T, 0	25	−500	1500	−3400,+2400	0.09
0, 7S	23	−300	1200	−2600,+2000	0.20
0, 7I	20	+200	1200	−2200,+2600	0.49

SD, standard deviation; N, nasal; T, temporal; I, inferior; S, superior; H, horizontal coordinate; V, vertical coordinate.
[a] Difference = single AO image cone density − wide-field AO montage cone density.
[b] Limits of agreement = 95% lower and upper bounds of the differences.
* Paired sample *t*-test.

We demonstrated wide limits of agreement between cone densities derived from gaze-directed single AO images and field projection on wide-field AO montage. Our data show a coefficient of variation (SD/mean) of around 10% in comparing the two sampling methods. There are a number of possible explanations for this. The first is misalignment between the retinal loci determined by gaze-direction and field projection on an AO montage. This is due to difference in position of the preferred retinal locus and the anatomic fovea as discussed above. However, our data and that of others[24] would suggest that the error in cone density measurement should not be as large as that shown by the wide limits of agreement because we only analyzed retinal loci between 3° and 7° where the gradient of change in cone density is only approximately 900 cones/mm^2 per degree of eccentricity (approximately 5% change) and most of the misalignment between the two methods was less than 1°.[25] The second explanation is variable cone visualization due to differences in image quality of the cropped sampling window derived from single AO images and the wide-field AO montage. Sampling windows from the latter would have been derived from two or more overlapping single AO images because these were taken at 1° to 2° apart. The optical Stiles Crawford effect has been shown to affect visualization of cones in AO images by way of changing the position at which the camera is focused over the pupil, so that previously dark spots on an AO frame become bright spots on subsequent AO frames when the camera is aligned at different positions over the pupil.[26] Thus, by overlapping two or more single AO images, a greater number of cone photoreceptors may be visualized as the optically silent nonwave guiding cones in one single AO frame becomes wave-guiding cones in another single AO image taken at slightly different gaze angles. This could account for the tendency for images obtained from sampling windows within the wide-field AO montage to show overall higher cone densities than those from single AO images at most of the study loci. An alternative explanation for this trend is that instead of improved visualization of cones, wide-field AO montage formed by potentially inaccurate stitching of overlapping single AO frames can result in a single cone appearing as two very closely spaced adjacent cones, thus resulting in overestimation of cone density. In certain individuals, the cone count from single AO images exceeded that from wide-field AO montage. This may occur if two separate cones are fused into a single cone during the process of imaging stitching. Another reason for reduced cone count in the wide-field AO montage is the introduction of noise into the montage by stitching together a poor quality single AO image with a good quality

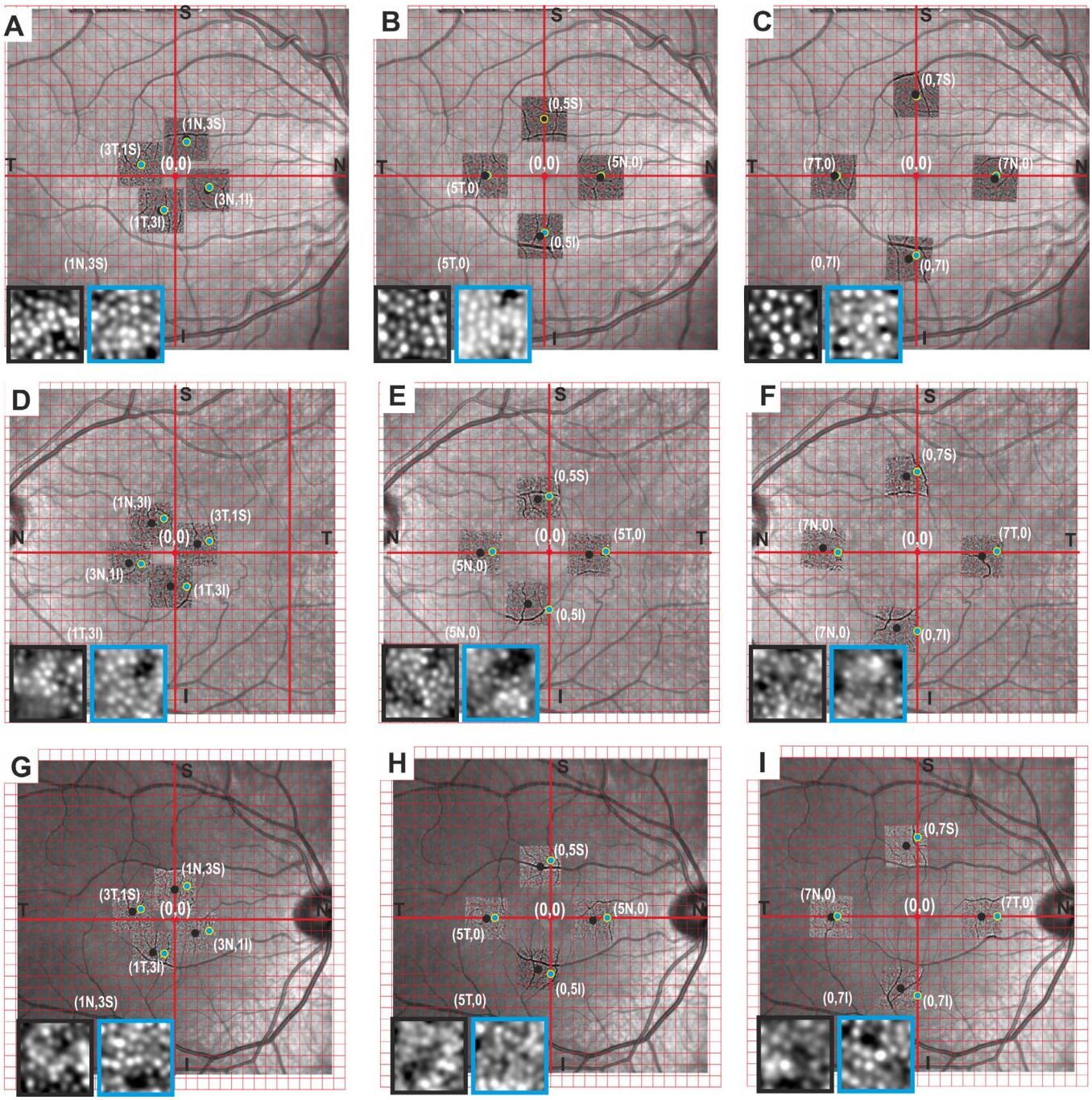

Figure 5. A Cartesian grid is overlaid onto the "30°" fundus image of each eye adjusted for magnification factor with its center at the location of that anatomical fovea determined from OCT. The discrepancies in gaze- (black dots) and field-derived (green dots) identification of retinal loci are shown in three cases. Subject 1 (D–F) and subject 16 (G–I) show temporal shift of gaze-derived loci compared to the field-derived loci, while subject 2 (A–C) shows nasal shift of the gaze-derived loci relative to the field-derived loci. Gaze-derived sampling windows from single AO frames are shown in the *black boxes*, while the field-derived sampling windows from compiled AO montages are shown in the *blue boxes*. The cone density values are shown in Table 4.

single AO image resulting in overall reduced cone visualization. This may contribute to poor image quality in sampling windows. It has been noted previously that image quality within an AO montage created by manual stitching of AO-SLO images may vary between different portions of the montage due to technical factors.[27] The open source MosaicJ montaging software that we use in our dataset assigns a

Table 4. Example of Three Cases Showing Discrepancy in Cone Density Between Gaze-Directed and Field-Determined Retinal Localization

	Cone Photoreceptor Cell Density, Cones/mm^2								
	Case 2, 29-yo			Case 1, 21-yo			Case 16, 67-yo		
LOCATION (H, V)	Wide-field AO Montage	Single AO Image	Difference[b]	Wide-field AO Montage	Single AO Image	Difference[b]	Wide-field AO Montage	Single AO Image	Difference[b]
1N, +3S	19,500	18,200	−1300	17,800	17,400	−400	16,900	15,800	−1200
3N, 1I	21,300	19,100	−2200	NA	NA	NA	16,100	16,100	0
1T, 3I	17,400	18,200	+900	17,100	13,500	−3600	NA	NA	NA
3T, 1S	21,300	22,100	+900	17,400	13,900	−3600	16,900	16,100	−800
5N, 0	19,500	16,500	−3000	15,000	16,700	+1800	17,700	15,400	−2300
5T, 0	18,700	18,200	−400	13,900	NA	NA	15,000	16,100	+1200
0, 5S	16,900	15,600	−1300	15,300	12,800	−2500	NA	NA	NA
0, 5I	16,500	15,200	−1300	13,200	13,900	+700	NA	NA	NA
7N, 0	17,400	15,200	−2200	13,900	13,200	−700	NA	NA	NA
7T, 0	16,100	15,600	−400	16,400	11,700	−4600	NA	14,200	NA
0, 7S	15,200	14,800	−400	11,700	12,500	+700	NA	NA	NA
0, 7I	16,100	13,500	−2600	NA	NA	NA	13,800	13,800	0
Mean Difference[a]			−1100***			−1400*			−500*

N, nasal; T, temporal; I, inferior; S, superior; H, horizontal coordinate; V, vertical coordinate; NA, not available due to poor sampling window image quality.

[a] Paired sample *t*-test.

[b] Difference = single AO image – wide-field AO montage.

* $P > 0.05$, ** $P < 0.05$, *** $P < 0.001$.

weighted contribution from each tile in regions of overlap.[28] The effect of this is demonstrated across six randomly chosen subjects in Supplementary Figure S2. In cases where the windows from each tile are of similar image quality, the window from the montage is of comparable contrast. In some cases, the windows from the contributing tiles are of varying quality, resulting in degradation of the quality of the window obtained from the montage versus that from the best tile. We did find a trend of a higher percentage of subjects (62% compared to 52%) with adequate sampling window quality at all 12 study loci when single AO frames were used for deriving cone densities but this was not statistically significant.

Previous reports of cone photoreceptor density calculated from AO images have estimated that at 3° eccentricity, the cone density is 16,000 – 21,000 cones/mm^2.[12,29] At a slightly greater eccentricity of 3.2° (at 3° horizontal and 1° vertical displacement), our results of 18,000 to 19,000 cones/mm^2 are in keeping with these previous measurements, with our study similarly demonstrating a tendency for higher cone density measurements in the temporal and nasal quadrants compared to the superior and inferior quadrants. As expected, our estimates of the average cone density decreased with increasing eccentricity from the fovea. Our cone density measurements at 5° eccentricity, 17,800 and 17,500 cones/mm^2 in the temporal and nasal quadrants, respectively, are within the estimates reported by Feng et al.,[12] which reported estimates of between 16,200 and 20,500 cones/mm^3 depending on which sampling method was used at that locus. At the superior and inferior quadrants, their estimates for cone density are between 14,100 and 19,200 cones/mm^3 and again our estimates of 16,500 and 16,200 cones/mm^3 fell within this range. The relative nasotemporal symmetry that we observed is consistent with results of previous AO imaging[25,27] and histological data[30]

Our study had a number of limitations. Firstly, the number of subjects analyzed was small and this may contribute to the wide limits of agreement. Nevertheless, the estimates of cone density and the pattern of cone density changes throughout the regions of the

macula studied were within the limits expected when comparing to data from previous reports. Secondly, we examined agreement in cone density measurements at 12 retinal loci within the central 14° field of the macula. The limits of agreement may not be applicable to other retinal loci. Thirdly, our data were derived from automatic calculations of cone densities without manual correction. It has been shown that the high variability seen in automated estimates of cone density can be reduced dramatically by manual correction of the automated cone identification.[25,31,32] Additionally, the determination of whether the sampling windows were of adequate image quality was subjective. Methods for defining image quality objectively have been described,[19,33] but it is known that using objective measures of image quality does not necessarily correlate with subjective assessment.[34] Whether the currently proposed methods of assessing image metrics are superior to subjective preference in selecting the most appropriate sampling window for accurately performing cone metrics remains to be investigated.

In conclusion, we illustrated a high frequency of poor quality sampling windows in a cohort of healthy subjects undergoing AO imaging. There was frequent misalignment between the center of gaze-directed single AO image and theoretical corresponding field-determined retinal loci. Although there was no overall bias in cone density between the two methods, wide limits of agreement were found. Future work is needed to determine the optimal method for alignment and merging the overlapping regions from single AO frames to generate the highest quality image and most reliable cone density measurements. Cone density values derived from these two methods are not interchangeable even in healthy subjects.

Acknowledgments

Supported in part by research grants from the Ophthalmic Research Institute of Australia (DMS, FKC); Global Ophthalmology Award Program Bayer (FKC); National Health & Medical Research Council (Early Career Fellowship; APP1054712, FKC); Retina Australia (FKC); and donations from the Miocevich, Constantine and Saleeba families (FKC) and the Health Department of Western Australia (FKC).

Disclosure: **A.L. Chew**, None; **D.M. Sampson**, None**; I. Kashani**, None; **F.K. Chen**, None

*ALC and DMS are equal first authors.

References

1. Lombardo M, Serrao S, Devaney N, et al. Adaptive optics technology for high-resolution retinal imaging. *Sensors (Basel)*. 2012;13:334–66.
2. Yuen T, Chui P, Song H, Burns SA. Adaptive-optics imaging of human cone photoreceptor distribution. *J Opt Soc Am A Opt Image Sci Vis*. 2008;25:3021–3029.
3. Supriya D, Shwetha M, Kiran Anupama K, et al. Structural and function correlation of cone packing utilizing adaptive optics and microperimetry. *Biomed Res Int*. 2015;2015:1–4.
4. Ratnam K, Carroll J, Porco TC, et al. Relationship between foveal cone structure and clinical measures of visual function in patients with inherited retinal degenerations. *Invest Ophthalmol Vis Sci*. 2013;54:5836–5847.
5. Cooper RF, Sulai YN, Dubis AM, et al. Effects of intraframe distortion on measures of cone mosaic geometry from adaptive optics scanning light ophthalmoscopy. *Transl Vis Sci Technol*. 2016;5:1–14.
6. Bennett AG, Rudnicka AR, Edgar DF. Improvements on Littmann's method of determining the size of retinal features by fundus photography. *Graefe's Arch Clin Exp Ophthalmol*. 1994;232:361–367.
7. Bukowska DM, Chew AL, Huynh E, et al. Semi-automated identification of cones in the human retina using circle Hough transform. *Biomed Opt Express*. 2015;6:4676–4693.
8. Thévenaz P, Unser M. User-friendly semiautomated assembly of accurate image mosaics in microscopy. *Microsc Res Tech*. 2007;70:135–46.
9. Pach J, Pennell DO, Romano PE. Optic disc photogrammetry: magnification factors for eye position, centration, and ametropias, refractive and axial; and their application in the diagnosis of optic nerve hypoplasia. *Ann Ophthalmol*. 1989;21:454–62.
10. Arnold JV, Gates JW, Taylor KM. Possible errors in the measurement of retinal lesions. *Invest Ophthalmol Vis Sci*. 1993;34:2576–80.
11. Debellemanière G, Flores M, Tumahai P, et al. Assessment of parafoveal cone density in patients taking hydroxychloroquine in the absence of clinically documented retinal toxicity. *Acta Ophthalmol*. 2015;93:e534–e540.
12. Feng S, Gale MJ, Fay JD, et al. Assessment of different sampling methods for measuring and representing macular cone density using flood-

illuminated adaptive optics. *Invest Ophthalmol Vis Sci*. 2015;56:5751–5763.
13. Li KY, Tiruveedhula P, Roorda A. Intersubject variability of foveal cone photoreceptor density in relation to eye length. *Invest Ophthalmol Vis Sci*. 2010;51:6858–6867.
14. Shemonski ND, South FA, Liu Y-Z, et al. Computational high-resolution optical imaging of the living human retina. *Nat Photonics*. 2015;9: 440–443.
15. South FA, Liu Y-Z, Carney PS, Boppart SA. Computed optical interferometric imaging: methods, achievements, and challenges. *IEEE J Sel Top Quantum Electron*. 2016;22:186–196.
16. Wong KSK, Jian Y, Cua M, et al. In vivo imaging of human photoreceptor mosaic with wavefront sensorless adaptive optics optical coherence tomography. *Biomed Opt Express*. 2015;6:580.
17. Putnam NM, Hofer HJ, Chen L, Williams DR. The locus of fixation and the foveal cone mosaic. *J Vis*. 2005:632–639.
18. Li KY, Tiruveedhula P, Roorda A. Intersubject variability of foveal cone photoreceptor density in relation to eye length. *Invest Ophthalmol Vis Sci*. 2010;51:6858–6867.
19. Lombardo M, Serrao S, Lombardo G, et al. Technical factors influencing cone packing density estimates in adaptive optics flood illuminated retinal images. *PLoS One*. 2014;9:e107402.
20. Zeffren BS, Applegate RA, Bradley A, Heuven WA van. Retinal fixation point location in the foveal avascular zone. *Invest Ophthalmol Vis Sci*. 1990;31:2099–2105.
21. Ditchburn RW. *Eye-Movements and Visual Perception*. xvi. New York: Clarendon (Oxford University Press); 1973.
22. Steinman RM. Effect of target size, luminance, and color on monocular fixation*. *J Opt Soc Am*. 1965;55:1158–1165.
23. Lombardo M, Lombardo G, Lomoriello DS, et al. Interocular symmetry of parafoveal photoreceptor cone density distribution. *Retina*. 2013;33: 1640–1649.
24. Song H, Yuen T, Chui P, et al. Variation of cone photoreceptor packing density with retinal eccentricity and age. *Invest Ophthalmol Vis Sci*. 2015: 7376–7384.
25. Lombardo M, Serrao S, Ducoli P, Lombardo G. Eccentricity dependent changes of density, spacing and packing arrangement of parafoveal cones. *Ophthalmic Physiol Opt*. 2013;33:516–526.
26. Miloudi C, Rossant F, Bloch I, et al. The Negative cone mosaic: a new manifestation of the optical stiles-crawford effect in normal eyes. *Invest Ophthalmol Vis Sci*. 2015;56:7043–7050.
27. Chui TY, Song H, Burns SA. Adaptive-optics imaging of human cone photoreceptor distribution. *J Opt Soc Am A*. 2008;25:3021–3029.
28. Thévenaz P, Unser M. User-friendly semiautomated assembly of accurate image mosaics in microscopy. *Microsc Res Tech*. 2007;70:135–146.
29. Dabir S, Mangalesh S, Kumar K a, et al. Variations in the cone packing density with eccentricity in emmetropes. *Eye*. 2014;28:1488–1493.
30. Curcio CA, Sloan KR, Kalina RE, Hendrickson AE. Human photoreceptor topography. *J Comp Neurol*. 1990;523:497–523.
31. Bidaut Garnier M, Flores M, Debellemanière G, et al. Reliability of cone counts using an adaptive optics retinal camera. *Clin Experiment Ophthalmol*. 2014;42:833–840.
32. Garrioch R, Langlo C, Dubis AM, et al. Repeatability of in vivo parafoveal cone density and spacing measurements. *Optom Vis Sci*. 2012; 89:632–643.
33. Ramaswamy G, Devaney N. Pre-processing, registration and selection of adaptive optics corrected retinal images. *Ophthalmic Physiol Opt*. 2013;33:527–539.
34. Gim G-Y, Kim H, Lee J-A, Kim W-Y. Subjective Image-Quality Estimation Based on Psychophysical Experimentation. In: *Advances in Image and Video Technology*. Berlin, Heidelberg: Springer Berlin Heidelberg; 2007:346–356.